

Cross-scale interaction of host tree size and climatic water deficit governs bark beetle-induced tree mortality

Michael J. Koontz^{1,2,3*}, Andrew M. Latimer^{1,2}, Leif A. Mortenson⁴, Christopher J. Fettig⁵, Malcolm P. North^{1,2,6}

¹Graduate Group in Ecology, University of California, Davis, CA, USA

²Department of Plant Sciences, University of California, Davis, CA, USA

³Earth Lab, University of Colorado-Boulder; Boulder, CO, USA

⁴USDA Forest Service, Pacific Southwest Research Station, Placerville, CA, USA

⁵USDA Forest Service, Pacific Southwest Research Station, Davis, CA, USA

⁶USDA Forest Service, Pacific Southwest Research Station, Mammoth Lakes, CA, USA

*Correspondence: michael.koontz@colorado.edu

Keywords: *Dendroctonus brevicomis*, disturbance, drones, *Pinus ponderosa*, Sierra Nevada, structure from motion, forest structure, climate change-type drought, macroecology, Gaussian process

Date report generated: November 05, 2020

Abstract

The recent Californian hot drought (2012-2016) precipitated unprecedented ponderosa pine (*Pinus ponderosa*) mortality, largely attributable to the western pine beetle (*Dendroctonus brevicomis*; WPB). Broad-scale climate conditions can directly shape tree mortality patterns, but mortality rates respond non-linearly to climate when local-scale forest characteristics influence the behavior of tree-killing bark beetles (e.g., WPB). To test for these cross-scale interactions, we conduct aerial drone surveys at 32 sites along a gradient of climatic water deficit (CWD) spanning 350 km of latitude and 1000 m of elevation in WPB-impacted Sierra Nevada forests. We map, measure, and classify over 450,000 trees within 9 km², validating measurements with coincident field plots. We find greater size, proportion, and density of ponderosa pine (the WPB host) increase host mortality rates, as does greater CWD. Critically, we find a CWD/host size interaction such that larger trees amplify host mortality rates in hot/dry sites. Management strategies for climate change adaptation should consider how bark beetle disturbances can depend on cross-scale interactions, which challenge our ability to predict and understand patterns of tree mortality.

28 Introduction

29 Bark beetles dealt the final blow to many of the nearly 150 million trees killed in the California hot drought
30 of 2012 to 2016 and its aftermath.¹ A harbinger of climate change effects to come, record high temperatures
31 exacerbated the drought,^{2,3} which increased water stress in trees,^{4,5} making them more susceptible to
32 colonization by bark beetles.^{6,7} Further, a century of fire suppression has enabled forests to grow into dense
33 stands, which can also make them more vulnerable to bark beetles.^{6,8,9} This combination of environmental
34 conditions and forest structural characteristics led to tree mortality events of unprecedented size across the
35 state.^{10,11}

36 Tree mortality exhibited a strong latitudinal and elevational gradient^{4,11} that can only be partially explained
37 by coarse-scale measures of environmental conditions (i.e., historic climatic water deficit; CWD) and current
38 forest structure (i.e., current regional basal area).¹¹ Progressive loss of canopy water content offers additional
39 insight into tree stress and mortality risk, but cannot ultimately resolve which trees are actually killed by
40 bark beetles or elucidate factors driving bark beetle population dynamics and spread.⁵ Bark beetles respond
41 to local forest characteristics in positive feedbacks that non-linearly alter tree mortality dynamics against a
42 background of environmental conditions that stress trees.^{12,13} Thus, an explicit consideration of local forest
43 structure and composition^{14,15} as well as its cross-scale interaction with regional climate conditions¹⁶ can
44 refine our understanding of tree mortality patterns from California's recent hot drought. The challenge of
45 simultaneously measuring the effects of both local-scale forest features (such as structure and composition)
46 and broad-scale environmental conditions (e.g., CWD) on forest insect disturbance leaves their interaction
47 effect relatively underexplored.^{14–17}

48 The ponderosa pine/mixed-conifer forests in California's Sierra Nevada region are characterized by regular bark
49 beetle disturbances, primarily by the influence of western pine beetle (*Dendroctonus brevicomis*; WPB) on its
50 host ponderosa pine (*Pinus ponderosa*).¹⁸ WPB is a primary bark beetle—its reproductive success is contingent
51 upon host tree mortality, which itself requires enough beetles to mass attack the host tree and overwhelm its
52 defenses.¹⁹ This Allee effect creates a strong coupling between beetle selection behavior of host trees and
53 host tree susceptibility to colonization.^{19–21} A key defense mechanism of conifers to bark beetle attack is to
54 flood beetle bore holes with resin, which physically expels colonizing beetles, can be toxic to the colonizers
55 and their fungi, and may interrupt beetle communication.^{22,23} Under normal conditions, weakened trees
56 with compromised defenses are the most susceptible to colonization and will be the main targets of primary
57 bark beetles like WPB.^{13,23,24} Under severe water stress however, many trees no longer have the resources
58 available to mount a defense.^{7,13} Drought,^{12,25–27} especially when paired with high temperatures,^{24,28–30} can
59 trigger increased bark beetle-induced tree mortality as average tree vigor declines. As the local population

60 density of beetles increases due to successful reproduction within spatially-aggregated susceptible trees, mass
61 attacks grow in size and become capable of overwhelming formidable tree defenses. Even large healthy trees
62 may be susceptible to colonization and mortality when beetle population density is high.^{13,23,24} Thus, water
63 stress and beetle population density interact to influence whether individual trees are susceptible to bark
64 beetles. When extreme or prolonged drought increases host tree vulnerability, bark beetle population growth
65 rates increase, then become self-amplifying as greater beetle densities make additional host trees prone to
66 successful mass attack.^{12,13,15,24}

67 WPB activity is strongly influenced by forest structure– the spatial arrangement and size distribution of trees–
68 and tree species composition. Taking forest structure alone, high-density forests are more prone to bark
69 beetle-induced tree mortality compared to thinned forests^{6,9} which may arise as greater competition for water
70 resources amongst crowded trees lowers average tree resistance,³¹ or because smaller gaps between trees protect
71 pheromone plumes from dissipation by the wind and thus enhance intraspecific beetle communication.³² Tree
72 size is another aspect of forest structure that affects bark beetle host selection behavior with smaller trees
73 tending to have lower capacity for resisting attack, but larger trees being more desirable targets on account
74 of their thicker phloem providing greater nutritional content.^{13,33–35} Throughout an outbreak, some bark
75 beetle species will collectively “switch” the preferred size of tree to attack in order to navigate this trade-off
76 between host susceptibility and host quality.^{13,21,36–39} Taking forest composition alone, WPB activity in the
77 Sierra Nevada mountain range of California is necessarily tied to the regional distribution of its exclusive host,
78 ponderosa pine.¹⁸ Colonization by primary bark beetles can also depend on the local relative frequencies of
79 tree species in forest stands, reflecting the more general pattern that specialist insect herbivory tends to be
80 lower in taxonomically diverse forests compared to monocultures.^{40,41}

81 The interaction between forest structure and composition at both stand- and tree- scales also drives WPB
82 activity. For instance, dense forest stands with high host availability may experience greater beetle-induced
83 tree mortality because dispersal distances between potential host trees are shorter, which reduces predation
84 of adults searching for hosts and facilitates higher rates of colonization.^{33,42,43} High host availability can also
85 reduce the chance of individual beetles wasting their limited resources flying to and landing on a non-host
86 tree.^{44,45} At a finer scale, a host tree’s defensive capacity can depend on its canopy position, with reduced
87 biochemical defenses in suppressed, crowded trees.⁴⁶ Coarse-scale measures of forest structure and composition
88 can therefore only partially explain mechanisms affecting bark beetle disturbance. Finer-grain information is
89 also needed that explicitly recognizes tree species, size, and local density, which better capture the ecological
90 processes underlying insect-induced tree mortality.^{28,36,38,39}

91 The vast spatial extent of WPB-induced tree mortality in the 2012 to 2016 California hot drought challenges

92 our ability to simultaneously consider how broad-scale environmental conditions may interact with local
93 forest structure and composition to affect the dynamic between bark beetle selection and colonization of host
94 trees, and host tree susceptibility to attack.^{15,47} Measuring local forest structure generally requires expensive
95 instrumentation^{4,48} or labor-intensive field surveys,^{14,15,49} which constrains survey extent and frequency.
96 Small, unhumanned aerial systems (sUAS) enable relatively fast and cheap remote imaging over hundreds of
97 hectares of forest, which can be used to measure complex forest structure and composition at the individual
98 tree scale with Structure from Motion (SfM) photogrammetry.^{50,51} The ultra-high, centimeter-scale resolution
99 of sUAS-derived measurements as well as the ability to incorporate vegetation reflectance can help overcome
100 challenges in species classification and dead tree detection inherent in other remote sensing methods, such
101 as airborne LiDAR.⁵² Distributing such surveys across an environmental gradient can overcome the data
102 acquisition challenge inherent in investigating phenomena with both a strong local- and a strong broad-scale
103 component.

104 We used sUAS-derived remote sensing images over a network of 32 sites in Sierra Nevada ponderosa pine/mixed-
105 conifer forests spanning 1000 m of elevation and 350 km of latitude¹⁴ covering a total of 9 km², to investigate
106 how broad-scale environmental conditions interacted with local forest structure and composition to shape
107 patterns of tree mortality during the cumulative tree mortality event of 2012 to 2018. We asked:

- 108 1. How does the proportion of the ponderosa pine host trees in a local area and average host tree size
109 affect WPB-induced tree mortality?
- 110 2. How does the density of all trees (hereafter “overall density”) affect WPB-induced tree mortality?
- 111 3. How does the total basal area of all trees (hereafter “overall basal area”) affect WPB-induced tree
112 mortality?
- 113 4. How does environmentally-driven tree moisture stress affect WPB-induced tree mortality?
- 114 5. How do the effects of forest structure, forest composition, and environmental condition interact to
115 influence WPB-induced tree mortality?

116 Here, we show that a greater local proportion of host trees (ponderosa pine) strongly increases the probability
117 of host mortality, with greater host density amplifying this effect. We also show that larger host trees
118 increase the probability of host mortality in accordance with well-known life history of WPB. Critically,
119 we find a strong interaction between host size and CWD such that larger trees exacerbate host mortality
120 rates in hot/dry sites. Our results demonstrate a cross-scale interaction in the response of WPB to local
121 forest structure and composition across an environmental gradient, which helps reconcile differences between

122 observed ecosystem-wide tree mortality patterns and predictions from models based on coarser-scale forest
 123 structure.

124 Results

125 Tree detection algorithm performance

126 We found that the experimental `lmfx` algorithm⁵³ with parameter values of `dist2d = 1` and `ws = 2.5`
 127 performed the best across 7 measures of forest structure as measured by Pearson’s correlation with ground
 128 data (Table 1).

Table 1: Correlation and differences between the best performing tree detection algorithm (`lmfx` with `dist2d = 1` and `ws = 2.5`) and the ground data. An asterisk next to the correlation or RMSE indicates that this value was within 5% of the value of the best-performing algorithm/parameter set. Ground mean represents the mean value of the forest metric across the 110 field plots that were visible from the sUAS-derived imagery. The median error is calculated as the median of the differences between the air and ground values for the 110 visible plots. Thus, a positive number indicates an overestimate by the sUAS workflow and a negative number indicates an underestimate.

Forest structure metric	Ground mean	Correlation with ground	RMSE	Median error
total tree count	19	0.67*	8.68*	2
count of trees > 15 m	9.9	0.43	7.38	0
distance to 1st neighbor (m)	2.8	0.55*	1.16*	0.26
distance to 2nd neighbor (m)	4.3	0.61*	1.70*	0.12
height (m); 25 th percentile	12	0.16	8.46	-1.2
height (m); mean	18	0.29	7.81*	-2.3
height (m); 75 th percentile	25	0.35	10.33*	-4

129 Classification accuracy for live/dead and host/non-host

130 The accuracy of live/dead classification on a withheld test dataset was 96.4%. The accuracy of species
 131 classification on a withheld testing dataset was 64.1%. The accuracy of WPB host/non-WPB-host (i.e.,
 132 ponderosa pine versus other tree species) on a withheld testing dataset was 71.8%.

133 Site summary based on best tree detection algorithm and classification

134 Across all study sites, we detected, segmented, and classified 452,413 trees in 23,187, 20 x 20m pixels (with
 135 the area of each pixel being approximately equivalent to that of a field plot). Of these trees, we classified
 136 118,879 as dead (26.3% mortality). Estimated site-level tree mortality ranged from 6.8% to 53.6%. See

137 Supplementary Information for site summaries and comparisons to site-level mortality measured from field
138 data.

139 **Effect of local structure and regional climate on tree mortality attributed to western pine**
140 **beetle**

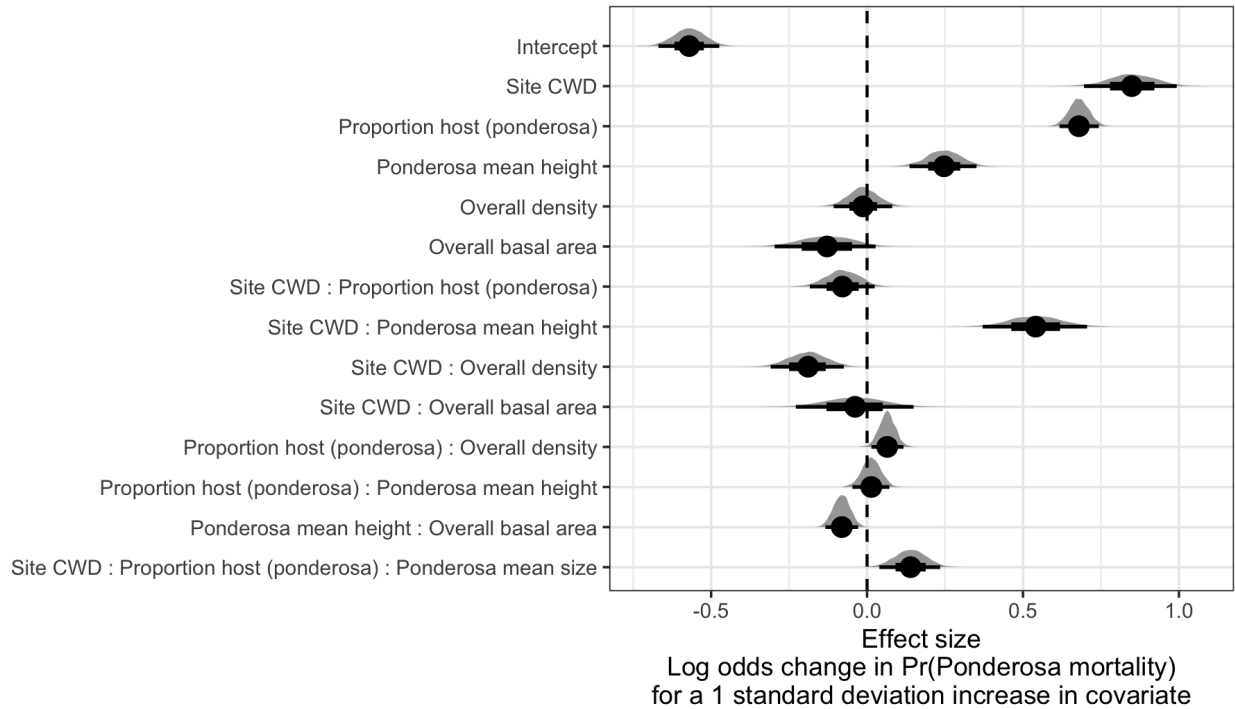


Figure 1: Posterior distributions of effect size from zero-inflated binomial model predicting the probability of ponderosa pine mortality in a 20 x 20-m cell given forest structure characteristics and site-level climatic water deficit (CWD). The gray filled area for each model covariate represents the probability density of the posterior distribution, the point underneath each density curve represents the median of the estimate, the bold interval surrounding the point estimate represents the 66% credible interval, and the thin interval surrounding the point estimate represents the 95% credible interval.

141 Site-level CWD exerted a positive main effect on the probability of ponderosa mortality (effect size: 0.85;
142 95% CI: [0.70, 0.99]; Figure 1). We found a positive main effect of proportion of host trees per cell (effect size:
143 0.68; 95% CI: [0.62, 0.74]), with a greater proportion of host trees (i.e., ponderosa pine) in a cell increasing
144 the probability of ponderosa pine mortality. We detected no effect of overall tree density nor overall basal
145 area (i.e., including both ponderosa pine and non-host species; tree density effect size: -0.01; 95% CI: [-0.11,
146 0.08]; basal area effect size: -0.13; 95% CI: [-0.29, 0.03]).

147 We found a positive two-way interaction between the overall tree density per cell and the proportion of trees
148 that were hosts, which is equivalent to a positive effect of the density of host trees (effect size: 0.06; 95% CI:
149 [0.01, 0.12]; Figure 1).

150 We found a positive main effect of mean height of ponderosa pine on the probability of ponderosa mortality
 151 (effect size: 0.25; 95% CI: [0.14, 0.35]). Coupled with the strong correlation between proportion of dead host
 152 trees and basal area killed (See Supplementary Figure 15), these results suggest that WPB attacked larger
 153 trees, on average. Further, there was a strong positive interaction between CWD and ponderosa pine mean
 154 height, such that larger trees were especially likely to increase the local probability of ponderosa mortality in
 155 hotter, drier sites (effect size: 0.54; 95% CI: [0.37, 0.70]; Figure 2).

156 We found no effect of the site-level CWD interactions with the proportion of host trees (effect size: -0.08;
 157 95% CI: [-0.18, 0.03]) nor of the interaction between CWD and total basal area (effect size: -0.04; 95% CI:
 158 [-0.23, 0.15]; Figure 1).

159 We found a negative effect of the CWD interaction with overall tree density (effect size: -0.19; 95% CI: [-0.31,
 160 -0.07]) as well as of the interaction between mean height of host trees and the overall basal area (effect size:
 161 -0.08; 95% CI: [-0.13, -0.03]; Figure 1).

162 While we found no interaction between proportion of host trees and mean host tree height, we did find a
 163 3-way interaction between these variables with CWD (effect size: 0.14; 95% CI: [0.04, 0.24]; Figure 1).

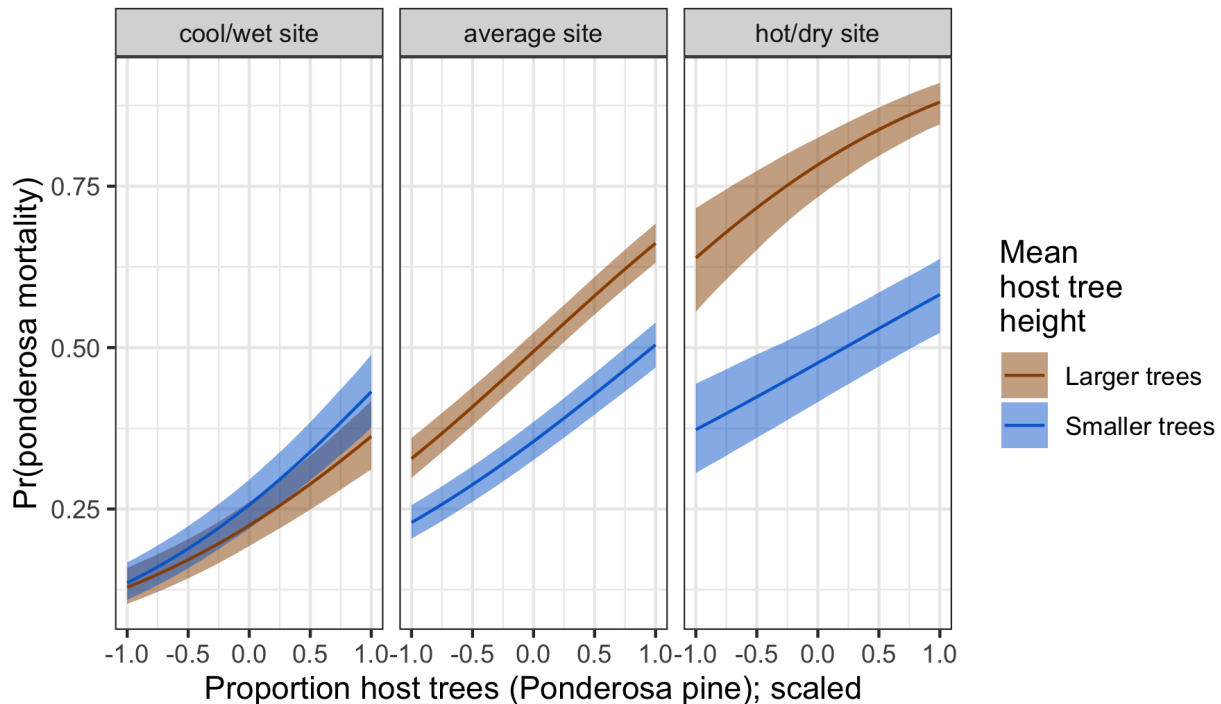


Figure 2: Line version of model results with 95% credible intervals showing primary influence of ponderosa pine structure on the probability of ponderosa pine mortality, and the interaction across climatic water deficit. The ‘larger trees’ line represents the mean height of ponderosa pine 0.7 standard deviations above the mean (approximately 24.1 m), and the ‘smaller trees’ line represents the mean height of ponderosa pine 0.7 standard deviations below the mean (approximately 12.1 m).

164 **Discussion**

165 This study uses drone-derived imagery to refine our understanding of the patterns of tree mortality following
166 the 2012 to 2016 California hot drought and its aftermath. By simultaneously measuring the effects of
167 local forest structure and composition across broad-scale environmental gradients, we were able to better
168 characterize the influence of a tree-killing insect, the WPB, compared to using correlates of tree stress alone.

169 **Strong positive main effect of CWD**

170 We found a strong positive effect of site-level CWD on ponderosa pine mortality rate. We did not measure
171 tree water stress at an individual tree level as in other recent work,¹⁵ and instead treated CWD as a general
172 indicator of tree stress following results of coarser-scale studies.¹¹ When measured at a fine scale, even if not
173 at an individual tree level, progressive canopy water loss can be a good indicator of tree water stress and
174 increased vulnerability to mortality from drought or bark beetles.⁵ Though our entire study area experienced
175 exceptional hot drought between 2012 and 2015,^{2,3} using a 30-year historic average of CWD as a site-level
176 indicator of tree stress doesn't allow us to disentangle whether water availability was lower in an absolute
177 sense during the drought or whether increasing tree vulnerability to bark beetles was driven by chronic water
178 stress at these historically hotter/drier sites.⁵⁴

179 **Positive effect of host proportion and density**

180 A number of mechanisms associated with the relative abundance of species in a local area might underlie the
181 strong effect of host proportion on the probability of host tree mortality. Frequency-dependent herbivory–
182 whereby mixed-species forests experience less herbivory compared to monocultures (as an extreme example)–
183 is common, especially for oligophagous insect species.⁴⁰ Nonhost volatiles reduce attraction of several species
184 of bark beetles to their aggregation pheromones,⁵⁵ including WPB.⁵⁶ Combinations of nonhost volatiles and
185 an antiaggregation pheromone have been used successfully to reduce levels of tree mortality attributed to
186 WPB in California.^{57,58} The positive relationship between host density and susceptibility to colonization by
187 bark beetles has been so well-documented at the experimental plot level^{43,59,60} that lowering stand densities
188 through selective harvest of hosts is commonly recommended for reducing future levels of tree mortality
189 attributed to bark beetles,⁶¹ including WPB.¹⁸ Greater host density shortens the flight distance required
190 for WPB to disperse to new hosts, which likely facilitates bark beetle spread, however we calibrated our
191 aerial tree detection to ~400 m² areas rather than to individual tree locations, so our data are insufficient to
192 address these relationships. Increased density of ponderosa pine, specifically, may disproportionately increase
193 the competitive environment for host trees (and thus increase their susceptibility to WPB colonization) if

194 intraspecific competition amongst ponderosa pine trees is stronger than interspecific competition as would
195 be predicted with coexistence theory.⁶² Finally, greater host densities increase the frequency that searching
196 WPB land on hosts, rather than nonhosts, thus reducing the amount of energy expended during host finding
197 and selection as well as the time that searching WPB spend exposed to a variety of predators outside the
198 host tree.

199 **No main effect of overall density, but interaction with CWD**

200 We detected no relationship between overall tree density and ponderosa pine mortality, though work from
201 the coincident ground plots showed a negative relationship.¹⁴ 28 also shows greater MPB infestation in
202 lower-density sites in Montana However, 31 and 14 found that measures of overall tree density explained
203 more variation in tree mortality than measures of host availability, though those conclusions were based on
204 broader-scale analyses³¹ or a different response variable.¹⁴

205 Our greater sample size may have enabled us to more finely parse the role of multi-faceted forest structure
206 and composition, along with CWD and interactions, in driving ponderosa pine mortality rates. Indeed, we
207 did find a negative two-way interaction between site CWD and overall density, suggesting denser stands
208 experienced lower rates of ponderosa mortality in hotter, drier sites, which comports with 9 in results from
209 their unmanipulated gradient of overall density in the same region during the same hot drought. In the
210 absence of active management, forest structure is largely a product of climate and, with increasing importance
211 at finer spatial scales, topographic conditions.⁶³ Denser forest patches in our study may indicate greater local
212 water availability, more favorable conditions for tree growth and survivorship, and increased resistance to
213 beetle-induced tree mortality, especially when denser patches are found in hot, dry sites.^{9,63,64}

214 **Effect of overall basal area**

215 While overall tree density is likely an indicator of favorable microsites in fire-suppressed forests, overall
216 basal area is a better indicator of the local competitive environment especially in water-limited forests.^{63,64}
217 However, we found no main effect of overall basal area on the probability of ponderosa mortality, nor of its
218 interaction with site-level CWD. This contrasts to the results from 11, and from analyses of coincident field
219 plots.¹⁴ While the contrast to 11 might be explained by different scales of analyses (i.e., 3500 x 3500 m pixels
220 vs. 20 x 20 m pixels), the contrast with the coincident ground plots is more puzzling. One explanation is that
221 the drone sampling captured more area beyond the conditionally-sampled field plots (i.e., 10% ponderosa
222 pine basal area mortality was a criterion for plot selection) that reflected a different relationship between
223 local basal area and tree mortality. Perhaps more likely is that our measure of total basal area isn't precise

224 enough to represent the local competitive environment compared to field-derived basal area. For our study,
225 basal area was derived from species-specific and inherently noisy allometric relationships with tree height,
226 which itself was derived from the SfM processing of drone imagery. As remote sensing technology improves
227 to enable finer-scale information extraction (e.g., individual tree measurements), more dialogue between
228 ecologists of all stripes^{65–67} is needed to fully imagine how to best measure natural phenomena remotely,
229 either by adopting wheels already invented or by innovating something brand new.

230 **Positive main effect of host tree mean size**

231 The positive main effect of host tree mean size on ponderosa mortality rates tracks the conventional wisdom
232 on the dynamics of WPB in the Sierra Nevada, as well as other primary bark beetles.¹⁸ WPB exhibit a
233 preference for trees 50.8 to 76.2 cm DBH,^{68,69} and a positive relationship between host tree size and levels of
234 tree mortality attributed to WPB was reported by 14 in the coincident field plots as well as in other recent
235 studies.^{9,15,70} Larger trees are more nutritious and are therefore ideal targets if local bark beetle density is
236 high enough to successfully initiate mass attack and overwhelm tree defenses, as can occur when many trees
237 are under severe water stress.^{7,13,24} In the recent hot drought, we expected that most trees would be under
238 severe water stress, setting the stage for increasing beetle density, successful mass attacks, and targeting of
239 larger trees. Given that our dead tree height calibration was conservative (accounting for underestimates of
240 drone-derived dead tree heights relative to field-measured trees), it is likely that the positive main effect of tree
241 height that we report represents a lower bounds of this effect. Additionally, 14 found no tree size/mortality
242 relationship for incense cedar or white fir in the coincident field plots. These species represent 22.3% of the
243 total tree mortality observed in their study, yet in our study all dead trees were classified as ponderosa pine
244 (see Methods) which could have further dampened the positive effect of tree size on tree mortality that we
245 identified.

246 **Cross-scale interaction of CWD and host tree size**

247 In hotter, drier sites, a larger average host size increased the probability of host mortality. Notably, a similar
248 pattern was shown by 65 in a study confined to the southern Sierra Nevada (i.e., the hottest, driest portion of
249 the more spatially extensive results we present here) with a strong positive tree height/mortality relationship
250 in areas with the greatest vapor pressure deficit and no tree height/mortality relationship in areas with the
251 lowest vapor pressure deficit. Our work suggests that the WPB was cueing into different aspects of forest
252 structure across an environmental gradient in a spatial context in a parallel manner to the temporal context
253 noted by 65 and 70, who observed that mortality was increasingly driven by larger trees as the hot drought
254 proceeded and became more severe. A temporal signal of bark beetles attacking larger and larger host trees

255 reflects the positive feedback between forest structure and bark beetle population dynamics as the population
256 phase cycles from endemic to epidemic.¹³ This positive feedback leading to eruptive population dynamics
257 is well-documented as a temporal phenomenon, and here we show a similar pattern in a spatial context
258 mediated through site-level CWD.

259 A key difference from the endemic-to-epidemic positive feedback noted by 13 is that none of our study areas
260 were considered to be in an endemic population phase by typical measures of WPB dynamics.^{31,33} WPB
261 dynamics at all sites were considered epidemic, with >5 trees killed per ha (see Supplementary Information).
262 The cross-scale interaction between broad-scale CWD and local-scale host tree size, even amongst populations
263 all in an epidemic phase, highlights the dramatic implications of the positive feedback for landscape-scale
264 tree mortality. The massive tree mortality in hotter/drier Sierra Nevada forests^{4,11} during the 2012 to 2016
265 hot drought likely arose as a synergistic alignment of environmental conditions and local forest structure
266 that allowed WPB to successfully colonize large trees, rapidly increase in population size, and expand. The
267 unexpectedly low mortality in cooler/wetter Sierra Nevada forests compared to model predictions based on
268 coarser-scale forest structure data¹¹ may result from a different WPB response to local forest structure due
269 to a lack of an alignment with favorable climate conditions and a weaker positive feedback.

270 **Limitations and future directions**

271 We have demonstrated that drones can be effective means of collecting forest data at multiple, vastly different
272 spatial scales to investigate a single, multi-scale phenomenon— from meters in between trees, to hundreds of
273 meters of elevation, to hundreds of thousands of meters of latitude. Some limitations remain, but can be
274 overcome with further refinements in the use of this tool for forest ecology. Most of these limitations arise
275 from classification and measurement of standing dead trees, making it imperative to work with field data for
276 calibration and uncertainty reporting.

277 The greatest limitation in our study arising from classification uncertainty is in the assumption that all dead
278 trees were ponderosa pine, which we estimate from coincident field plots is true approximately 73.4% of the
279 time. Because the forest structure factors influencing the likelihood of individual tree mortality during the hot
280 drought depended on tree species,¹⁵ we cannot rule out that some of the ponderosa pine mortality relationships
281 to forest structure that we observed may be partially explained by those relationships in other species that
282 were misclassified as ponderosa pine using our methods. However, the overall community composition across
283 our study area was similar¹⁴ and we are able to reproduce similar forest structure/mortality patterns in
284 drone-derived data when restricting the scope of analysis to only trees detected in the footprints of the
285 coincident field plots (see Supplementary Information). Thus, we remain confident that the patterns we

286 observed were driven primarily by the dynamic between WPB and ponderosa pine. While spectral information
287 of foliage could help classify living trees to species, the species of standing dead trees were not spectrally
288 distinct. This challenge of classifying standing dead trees to species implies that a conifer forest systems with
289 less bark beetle and tree host diversity, such as mountain pine beetle outbreaks in relative monocultures of
290 naturally-occurring lodgepole pine forests in the Intermountain West, should be particularly amenable to the
291 methods presented here even with minimal further refinement because dead trees will almost certainly belong
292 to a single species and have succumbed to colonization by a single bark beetle species. For similar reasons,
293 these methods would also work particularly well if imagery were also captured prior to the mortality event.

294 Some uncertainty surrounded our ability to detect trees using the geometry of the dense point clouds derived
295 with SfM. The horizontal accuracy (i.e., longitude/latitude position) of the tree detection was better than the
296 vertical accuracy (i.e., height), which may result from a more significant error contribution by the field-based
297 calculations of tree height compared to tree position relative to plot center (Table 1). Height measurements
298 were particularly challenging for standing dead trees, because SfM can fail to produce any points representing
299 narrow, needleless treetops in the resulting dense point cloud. Our conservative calibration of drone-measured
300 tree heights to field-measured heights strengthened the main effect of CWD on host mortality in our model
301 and reversed the effect of host tree height (see Supplementary Information). We report that larger host trees
302 increase the probability of host tree mortality, while models using uncalibrated tree heights show that larger
303 trees decrease host mortality rates (see Supplementary Information). While our live/dead classification was
304 fairly accurate (96.4% on a withheld dataset), our species classifier would likely benefit from better crown
305 segmentation because the pixel-level reflectance values within each crown are averaged to characterize the
306 “spectral signature” of each tree. With better delineation of each tree crown, the mean value of pixels within
307 each tree crown will likely be more representative of that tree’s spectral signature.

308 Better tree detection, crown segmentation, and dead tree height measurement would likely improve with
309 better SfM point clouds which can be enhanced with greater overlap between images⁷¹ or with oblique (i.e.,
310 off-nadir) imagery.⁷² 71 found that 95% overlap was preferable for generating dense point clouds in forested
311 areas, and 72 reduced dense point cloud errors using imagery taken at 30 degrees off-nadir. We only achieved
312 91.6% overlap with the X3 RGB camera and 83.9% overlap with the multispectral camera, and all imagery
313 was nadir-facing. We anticipate that computer vision and deep learning will also prove helpful in overcoming
314 some of these detection and classification challenges.⁷³

315 Finally, we note our study is constrained by the uncertainty in measuring basal area from SfM processing of
316 drone-derived imagery. This uncertainty makes it challenging to represent typical field-based measures of
317 local competitive environment (e.g., total plot basal area) or ecosystem impact (e.g., proportion of dead basal

318 area in a plot) in a statistical analysis. Instead, we opted to use the probability of ponderosa mortality as
319 our key response variable, which is well-suited to understanding the dynamics between WPB colonization
320 behavior and host tree susceptibility.

321 **Conclusions**

322 Climate change adaptation strategies emphasize management action that considers whole-ecosystem responses
323 to inevitable change,⁷⁴ which requires a macroecological understanding of how phenomena at multiple
324 scales can interact. Tree vulnerability to environmental stressors presents only a partial explanation for
325 tree mortality patterns during hot droughts, especially when bark beetles are present. We've shown that
326 drones can be a valuable tool for investigating multi-scalar phenomena, such as how local forest structure
327 combines with environmental conditions to shape forest insect disturbance. Understanding the conditions
328 that drive dry western U.S. forest responses to disturbances such as bark beetle outbreaks will be vital for
329 predicting outcomes from increasing disturbance frequency and intensity exacerbated by climate change.⁷⁵
330 Our study suggests that outcomes will depend on interactions between local forest structure and broad-scale
331 environmental gradients, with the potential for cross-scale interactions to enhance our understanding of forest
332 insect dynamics.

333 **Methods**

334 **Study system**

335 We designed the aerial survey to coincide with 160 vegetation/forest insect monitoring plots at 32 sites
336 established between 2016 and 2017 by 14 (Figure 3). The study sites were chosen to reflect typical west-side
337 Sierra Nevada yellow pine/mixed-conifer forests and were dominated by ponderosa pine.¹⁴ Sites were placed
338 in WPB-attacked, yellow pine/mixed-conifer forests across the Eldorado, Stanislaus, Sierra and Sequoia
339 National Forests and were stratified by elevation (914-1219 m, 1219-1524 m, 1524-1829 m above sea level). In
340 the Sequoia National Forest, the southernmost National Forest in our study, sites were stratified with the
341 lowest elevation band of 1219-1524 m and extended to an upper elevation band of 1829-2134 m to capture a
342 more similar forest community composition as at the more northern National Forests. The sites have variable
343 forest structure and plot locations were selected in areas with >35% ponderosa pine basal area and >10%
344 ponderosa pine mortality. At each site, five 0.041-ha circular plots were installed along transects with 80
345 to 200m between plots. In the field, 14 mapped all stem locations relative to the center of each plot using
346 azimuth/distance measurements. Tree identity to species, tree height, and diameter at breast height (DBH)
347 were recorded if DBH was greater than 6.35cm. Year of mortality was estimated based on needle color and

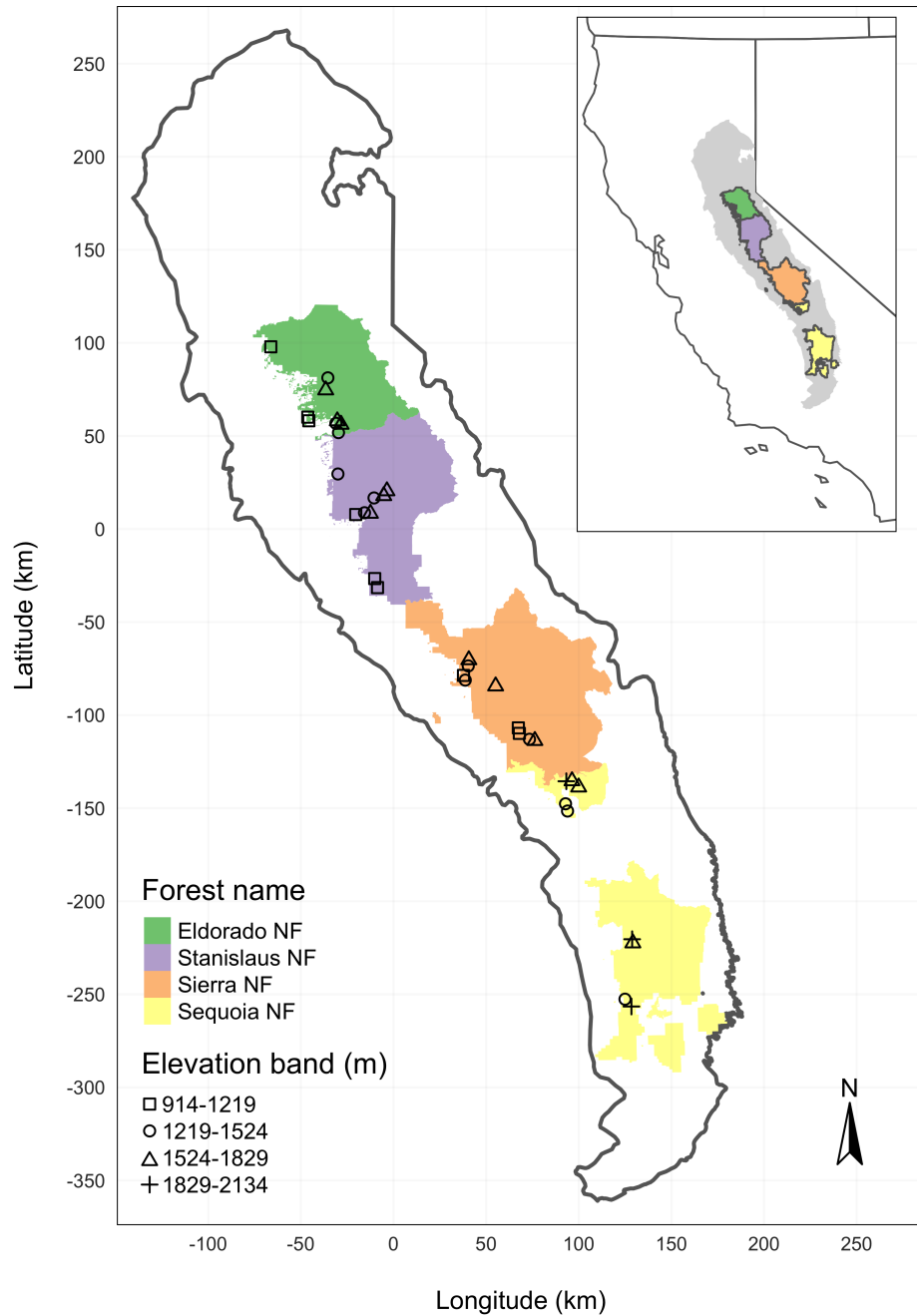


Figure 3: The network of field plots spanned a 350-km latitudinal gradient from the Eldorado National Forest in the north to the Sequoia National Forest in the south. Plots were stratified by three elevation bands in each forest, with the plots in the Sequoia National Forest (the southern-most National Forest) occupying elevation bands 305 m above the three bands in the other National Forests in order to capture a similar community composition.

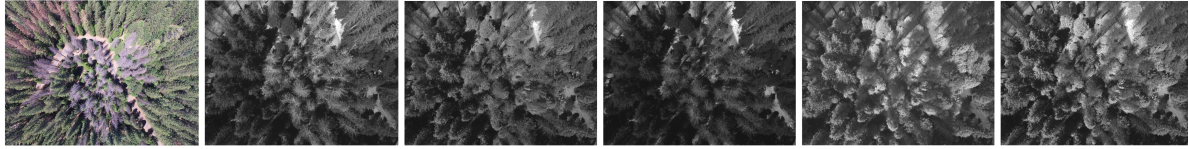
348 retention if it occurred prior to plot establishment, and was directly observed thereafter during annual site
349 visits. A small section of bark (approximately 625 cm²) on both north and south aspects was removed from
350 dead trees to determine if bark beetle galleries were present. The shape, distribution, and orientation of
351 galleries are commonly used to distinguish among bark beetle species.¹⁸ In some cases, deceased bark beetles
352 were present beneath the bark to supplement identifications based on gallery formation. During the spring
353 and early summer of 2018, all field plots were revisited to assess whether dead trees had fallen.¹⁴

354 In the typical life cycle of WPBs, females initiate host colonization by tunneling through the outer bark and
355 into the phloem and outer xylem where they rupture resin canals. As a result, oleoresin exudes and collects on
356 the bark surface, as is commonly observed with other bark beetle species. During the early stages of attack,
357 females release an aggregation pheromone component which, in combination with host monoterpenes released
358 from pitch tubes, is attractive to conspecifics.⁷⁶ An antiaggregation pheromone component is produced during
359 latter stages of host colonization by several pathways, and is thought to reduce intraspecific competition
360 by altering adult behavior to minimize overcrowding of developing brood within the host.⁷⁷ Volatiles from
361 several nonhosts sympatric with ponderosa pine have been demonstrated to inhibit attraction of WPB to
362 its aggregation pheromones.^{56,78} In California, WPB generally has 2-3 generations in a single year and can
363 often outcompete other primary bark beetles such as the mountain pine beetle in ponderosa pines, especially
364 in larger trees.³³ WPB population growth rates can, however, be reduced by competition with other beetle
365 species cohabitating in the same host tree, as well as by predation during dispersal to seek a host.³³

366 **Aerial data collection and processing**

367 Nadir-facing imagery was captured using a gimbal-stabilized DJI Zenmuse X3 broad-band red/green/blue
368 (RGB) camera⁷⁹ and a fixed-mounted Micasense Rededge3 multispectral camera with five narrow bands⁸⁰ on
369 a DJI Matrice 100 aircraft.⁸¹ Imagery was captured from both cameras along preprogrammed aerial transects
370 over ~40 ha surrounding each of the 32 sites (each of these containing five field plots) and was processed in a
371 series of steps to yield local forest structure and composition data suitable for our statistical analyses. All
372 images were captured in 2018 during a 3-month period between early April and early July, and thus our work
373 represents a postmortem investigation into the drivers of cumulative tree mortality. Following the call by 82,
374 we establish “data product levels” to reflect the image processing pipeline from raw imagery (Level 0) to
375 calibrated, fine-scale forest structure and composition information on regular grids (Level 4), with each new
376 data level derived from levels below it. Here, we outline the steps in the processing and calibration pipeline
377 visualized in Figure 4, and include additional details in the Supplementary Information.

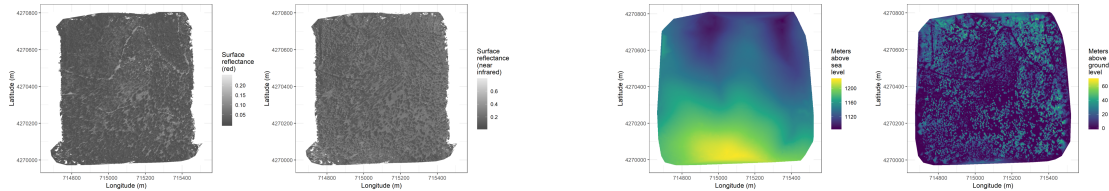
Level 0: raw data from sensors



Level 1: basic outputs from photogrammetric processing



Level 2: corrected outputs from photogrammetric processing

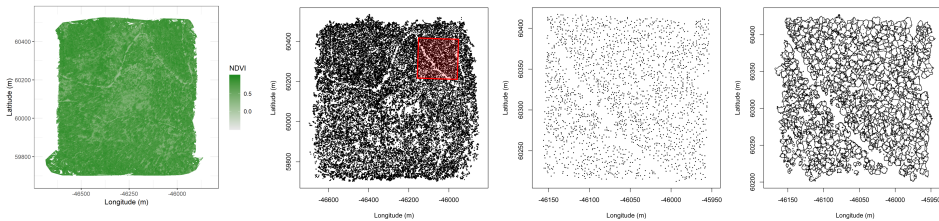


radiometric (e.g., normalize for atmosphere)

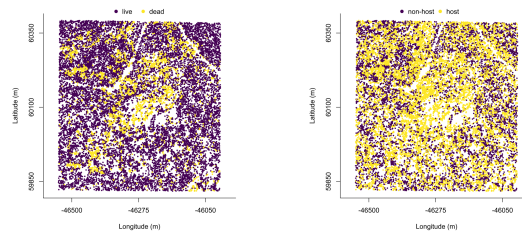
geometric (e.g., normalize for terrain)

Level 3: domain-specific information extraction

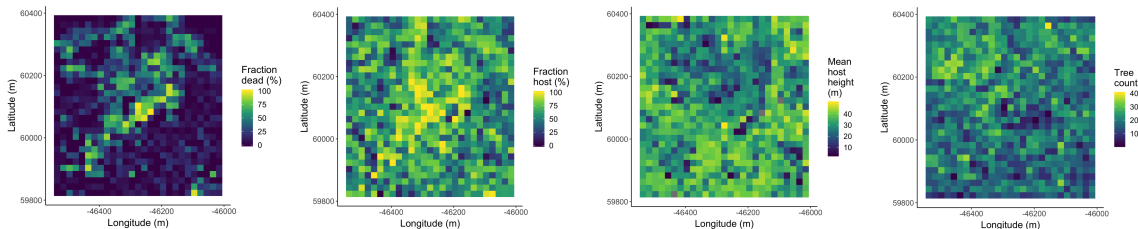
L3a
spectral
OR
geometric



L3b
spectral
AND
geometric



Level 4: aggregations to regular grids



379 Figure 4. Schematic of the data processing workflow for a single site with each new data product level derived
380 from data at lower levels. Level 0 represents raw data from the sensors. From left to right: RGB photo from
381 DJI Zenmuse X3, output images from Micasense Rededge3 (blue, green, red, near infrared, red edge). Level 1
382 represents basic outputs from the SfM workflow. From left to right: dense point cloud, RGB orthophoto,
383 digital surface model (DSM; ground elevation plus vegetation height). Level 2 represents radiometrically
384 or geometrically corrected Level 1 products. From left to right: radiometrically-corrected “red” surface
385 reflectance map, radiometrically-corrected “near infrared” surface reflectance map, digital terrain model
386 (DTM) derived by a geometric correction of the dense point cloud, canopy height model (CHM; DSM - DTM).
387 Level 3 represents domain-specific information extraction from Level 2 products and is divided into two
388 sub-levels. Level 3a products are derived using only spectral or only geometric data. From left to right: map
389 of Normalized Difference Vegetation Index,⁸³ map of detected trees derived from the CHM, detected trees
390 within red polygon, polygons representing segmented tree crowns within red polygon. Level 3b products are
391 derived using both spectral and geometric data. From left to right: trees classified as alive or dead based
392 on spectral reflectance within each segmented tree crown, trees classified as WPB host/non-host. Level 4
393 represents aggregations of Level 3 products to regular grids that better reflects the grain size of the validation
394 (e.g., to match area of validation field plots) or which provides neighborhood- rather than individual-scale
395 information (e.g., stand-level proportion of host trees). From left to right: grid representing fraction of dead
396 trees per cell, grid representing fraction of hosts per cell, grid representing mean host height per cell, tree
397 density per cell. All cells measure 20 x 20 m.

398 **Level 0: Raw data from sensors**

399 Raw data comprised approximately 1900 images per camera lens (one broad-band RGB lens and five narrow-
400 band multispectral lenses) for each of the 32 sites (Figure 4; Level 0). Prior to the aerial survey, two strips of
401 bright orange drop cloth (~100 x 15 cm) were positioned as an “X” over the permanent monuments marking
402 the center of the 5 field plots from 14 (see Supplementary Information).

403 We preprogrammed north-south aerial transects using Map Pilot for DJI on iOS flight software⁸⁴ at an
404 altitude of 120 m above ground level (with “ground” defined using a 1-arc-second digital elevation model⁸⁵).
405 The resulting ground sampling distance was approximately 5 cm/px for the Zenmuse X3 RGB camera and
406 approximately 8 cm/px for the Rededge3 multispectral camera. We used 91.6% image overlap (both forward
407 and side) at the ground for the Zenmuse X3 RGB camera and 83.9% overlap (forward and side) for the
408 Rededge3 multispectral camera.

409 **Level 1: Basic outputs from photogrammetric processing**

410 We used SfM photogrammetry implemented in Pix4Dmapper Cloud (www.pix4d.com) to generate dense point
411 clouds (Figure 4; Level 1, left), orthophotos (Figure 4; Level 1, center), and digital surface models (Figure 4;
412 Level 1, right) for each field site.⁷¹ For 29 sites, we processed the Rededge3 multispectral imagery alone to
413 generate these products. For three sites, we processed the RGB and the multispectral imagery together to
414 enhance the point density of the dense point cloud. All SfM projects resulted in a single processing “block,”
415 indicating that all images in the project were optimized and processed together. The dense point cloud
416 represents x, y, and z coordinates as well as the color of millions of points per site. The orthophoto represents
417 a radiometrically uncalibrated, top-down view of the survey site that preserves the relative x-y positions of
418 objects in the scene. The digital surface model is a rasterized version of the dense point cloud that shows
419 the altitude above sea level for each pixel in the scene at the ground sampling distance of the camera that
420 generated the Level 0 data.

421 **Level 2: Corrected outputs from photogrammetric processing**

422 **Radiometric corrections** A radiometrically-corrected reflectance map (Figure 4; Level 2, left two figures;
423 i.e., a corrected version of the Level 1 orthophoto) was generated using the Pix4D software by incorporating
424 incoming light conditions for each narrow band of the Rededge3 camera (captured simultaneously with the
425 Rededge3 camera using an integrated downwelling light sensor) as well as a pre-flight image of a calibration
426 panel of known reflectance (see Supplementary Information for camera and calibration panel details).

427 **Geometric corrections** We implemented a geometric correction to the Level 1 dense point cloud and
428 digital surface model by normalizing these data for the terrain underneath the vegetation. We generated the
429 digital terrain model representing the ground underneath the vegetation at 1-m resolution (Figure 4; Level
430 2, third image) by classifying each survey area’s dense point cloud into “ground” and “non-ground” points
431 using a cloth simulation filter algorithm⁸⁶ implemented in the `lidR`⁵³ package and rasterizing the ground
432 points using the `raster` package.⁸⁷ We generated a canopy height model (Figure 4; Level 2, fourth image) by
433 subtracting the digital terrain model from the digital surface model.

434 **Level 3: Domain-specific information extraction**

435 **Level 3a: Data derived from spectral or geometric Level 2 product** Using just the spectral
436 information from the radiometrically-corrected reflectance maps, we calculated several vegetation indices
437 including the normalized difference vegetation index [NDVI; 83; Figure 4; Level 3a, first image], the normalized
438 difference red edge,⁸⁸ the red-green index,⁸⁹ the red edge chlorophyll index,⁹⁰ and the green chlorophyll

Table 2: Algorithm name, number of parameter sets tested for each algorithm, and references.

Algorithm	Parameter sets tested	Reference(s)
li2012	131	91; 92; 93
lmfx	30	94
localMaxima	6	53
multichm	1	95
ptrees	3	96
vwf	3	97
watershed	3	98

440 Using just the geometric information from the canopy height model or terrain-normalized dense point cloud,
441 we generated maps of detected trees (Figure 4; Level 3a, second and third images) by testing a total of 7
442 automatic tree detection algorithms and a total of 177 parameter sets (Table 2). We used the field plot data
443 to assess each tree detection algorithm/parameter set by converting the distance-from-center and azimuth
444 measurements of the trees in the field plots to x-y positions relative to the field plot centers distinguishable in
445 the Level 2 reflectance maps as the orange fabric X’s that we laid out prior to each flight. In the reflectance
446 maps, we located 110 out of 160 field plot centers while some plot centers were obscured due to dense
447 interlocking tree crowns or because a plot center was located directly under a single tree crown. For each of
448 the 110 field plots with identifiable plot centers– the “validation field plots”, we calculated 7 forest structure
449 metrics using the ground data collected by 14: total number of trees, number of trees greater than 15 m
450 in height, mean height of trees, 25th percentile tree height, 75th percentile tree height, mean distance to
451 nearest tree neighbor, and mean distance to second nearest neighbor. For each tree detection algorithm and
452 parameter set described above, we calculated the same set of 7 structure metrics within the footprint of the
453 validation field plots. We calculated the Pearson’s correlation and root mean square error (RMSE) between
454 the ground data and the aerial data for each of the 7 structure metrics for each of the 177 automatic tree
455 detection algorithms/parameter sets. For each algorithm and parameter set, we calculated its performance
456 relative to other algorithms as whether its Pearson’s correlation was within 5% of the highest Pearson’s
457 correlation as well as whether its RMSE was within 5% of the lowest RMSE. We summed the number of
458 forest structure metrics for which it reached these 5% thresholds for each algorithm/parameter set. For
459 automatically detecting trees across the whole study, we selected the algorithm/parameter set that performed

460 well across the most forest metrics (see Results).

461 We delineated individual tree crowns (Figure 4; Level 3a, fourth image) with a marker controlled watershed
462 segmentation algorithm⁹⁹ implemented in the `ForestTools` package⁹⁷ using the detected treetops as markers.
463 If the automatic segmentation algorithm failed to generate a crown segment for a detected tree (e.g., often
464 snags with a very small crown footprint), a circular crown was generated with a radius of 0.5 m. If the
465 segmentation generated multiple polygons for a single detected tree, only the polygon containing the detected
466 tree was retained. Because image overlap decreases near the edges of the overall flight path and reduces the
467 quality of the SfM processing in those areas, we excluded segmented crowns within 35 m of the edge of the
468 survey area. Given the narrower field of view of the Rededge3 multispectral camera versus the X3 RGB
469 camera whose optical parameters were used to define the ~40 ha survey area around each site, as well as the
470 35 m additional buffering, the survey area at each site was ~30 ha (see Supplementary Information).

471 **Level 3b: Data derived from spectral and geometric information** We overlaid the segmented
472 crowns on the reflectance maps from 20 sites spanning the latitudinal and elevation gradient in the study.
473 Using QGIS (<https://qgis.org/en/site/>), we hand classified 564 trees as live/dead and as one of 5 dominant
474 species in the study area (ponderosa pine, *Pinus lambertiana*, *Abies concolor*, *Calocedrus decurrens*, or *Quercus*
475 *kelloggi*) using the mapped ground data as a guide. Each tree was further classified as “host” for ponderosa
476 pine or “non-host” for all other species.¹⁸ We extracted all the pixel values within each segmented crown
477 polygon from the five, Level 2 orthorectified reflectance maps (one per narrow band on the Rededge3 camera)
478 as well as from the five, Level 3a vegetation index maps using the `velox` package.¹⁰⁰ For each crown polygon,
479 we calculated the mean value of the extracted Level 2 and Level 3a pixels and used them as ten independent
480 variables in a five-fold cross validated boosted logistic regression model to predict whether the hand classified
481 trees were alive or dead. For just the living trees, we similarly used all 10 mean reflectance values per crown
482 polygon to predict tree species using a five-fold cross validated regularized discriminant analysis. The boosted
483 logistic regression and regularized discriminant analysis were implemented using the `caret` package in R.¹⁰¹
484 We used these models to classify all tree crowns in the data set as alive or dead (Figure 4; Level 3b, first
485 image) as well as the species of living trees (Figure 4; Level 3b, second image).

486 Because the tops of dead, needle-less trees are narrow, they may not be well-represented in the point
487 clouds produced using SfM photogrammetry, which biases their height estimates downward. Further, field
488 measurements can overestimate the heights of live trees relative to aerial survey methods.¹⁰² To correct these
489 measurement biases, we calibrated aerial tree height measurements to ground-based height measurements.
490 Specifically, we identified the crowns of 451 field-measured trees in the drone-derived tree data, modeled the

491 relationship between field- and drone-measured tree heights for both live and dead trees, and used the models
492 to adjust the drone-measured tree heights (See Supplementary Methods). We applied a conservative height
493 correction to live and dead trees based on trees measured by the drone to be greater than 20 m in height
494 that increased dead tree height by an average of 2.8 m and reduced the heights of live trees by an average of
495 0.9 m (See Supplementary Methods). Finally, we estimated the basal area of each tree from their corrected
496 drone-measured height using species-specific simple linear regressions of the relationship between height and
497 DBH as measured in the coincident field plots from 14.

498 **Level 4: Aggregations to regular grids**

499 We rasterized the forest structure and composition data at a spatial resolution similar to that of the field
500 plots to better match the grain size at which we validated the automatic tree detection algorithms. In each
501 raster cell, we calculated: number of dead trees, number of ponderosa pine trees, total number of trees, and
502 mean height of ponderosa pine trees. The values of these variables in each grid cell and derivatives from
503 them were used for visualization and modeling. Here, we show the fraction of dead trees per cell (Figure 4;
504 Level 4, first image), the fraction of host trees per cell (Figure 4; Level 4, second image), the mean height of
505 ponderosa pine trees in each cell (Figure 4; Level 4, third image), and the total count of trees per cell (Figure
506 4; Level 4, fourth image).

507 **Note on assumptions about dead trees**

508 For the purposes of this study, we assumed that all dead trees were ponderosa pine and thus hosts colonized
509 by WPB. This is a reasonably good assumption for our study area; for example, 14 found that 73.4% of dead
510 trees in their coincident field plots were ponderosa pine. Mortality was concentrated in the larger-diameter
511 classes and attributed primarily to WPB.¹⁴ The species contributing to the next highest proportion of dead
512 trees was incense cedar which represented 18.72% of the dead trees in the field plots. While the detected
513 mortality is most likely to be ponderosa pine killed by WPB, it is critical to interpret our results with these
514 limitations in mind.

515 **Environmental data**

516 We used CWD¹⁰³ from the 1981-2010 mean value of the basin characterization model¹⁰⁴ as an integrated
517 measure of historic temperature and moisture conditions for each of the 32 sites. Higher values of CWD
518 correspond to historically hotter, drier conditions and lower values correspond to historically cooler, wetter
519 conditions. CWD has been shown to correlate well with broad patterns of tree mortality in the Sierra
520 Nevada¹¹ as well as bark beetle-induced tree mortality.¹⁰⁵ The forests along the entire CWD gradient used in

521 this study experienced exceptional hot drought between 2012 to 2016 with a severity of at least a 1,200-year
522 event, and perhaps more severe than a 10,000-year event.^{2,3} We converted the CWD value for each site into a
523 z-score representing that site’s deviation from the mean CWD across the climatic range of Sierra Nevada
524 ponderosa pine as determined from 179 herbarium records described in 106. Thus, a CWD z-score of 1 would
525 indicate that the CWD at that site is one standard deviation hotter/drier than the mean CWD across all
526 geolocated herbarium records for ponderosa pine in the Sierra Nevada.

527 **Statistical model**

528 We used a generalized linear model with a zero-inflated binomial response and a logit link to predict the
529 probability of ponderosa pine mortality within each 20 x 20-m cell using the total number of ponderosa
530 pine trees in each cell as the number of trials, and the number of dead trees in each cell as the number of
531 “successes”. As covariates, we used the proportion of trees that are WPB hosts (i.e., ponderosa pine) in each
532 cell, the mean height of ponderosa pine trees in each cell, the count of trees of all species (overall density) in
533 each cell, and the site-level CWD using Eq. 1. Note that the two-way interaction between the overall density
534 and the proportion of trees that are hosts is directly proportional to the number of ponderosa pine trees in
535 the cell. We centered and scaled all predictor values, and used weakly-regularizing default priors from the
536 `brms` package.¹⁰⁷ To measure and account for spatial autocorrelation underlying ponderosa pine mortality,
537 we subsampled the data at each site to a random selection of 200, 20 x 20-m cells representing approximately
538 27.5% of the surveyed area. Additionally with these subsampled data, we included a separate exact Gaussian
539 process term per site of the noncentered/nonscaled interaction between the x- and y-position of each cell
540 using the `gp()` function in the `brms` package.¹⁰⁷ The Gaussian process estimates the spatial covariance in the
541 response variable (log-odds of ponderosa pine mortality) jointly with the effects of the other covariates.

$$y_{i,j} \sim \begin{cases} 0, & p \\ \text{Binom}(n_i, \pi_i), & 1 - p \end{cases}$$

$$\begin{aligned} \text{logit}(\pi_i) = & \beta_0 + \\ & \beta_1 X_{cwd,j} + \beta_2 X_{propHost,i} + \beta_3 X_{PipoHeight,i} + \\ & \beta_4 X_{overallDensity,i} + \beta_5 X_{overallBA,i} + \\ & \beta_6 X_{cwd,j} X_{PipoHeight,i} + \beta_7 X_{cwd,j} X_{propHost,i} + \\ & \beta_8 X_{cwd,j} X_{overallDensity,i} + \beta_9 X_{cwd,j} X_{overallBA,i} + \\ & \beta_{10} X_{propHost,i} X_{PipoHeight,i} + \beta_{11} X_{propHost,i} X_{overallDensity,i} + \\ & \beta_{12} X_{PipoHeight,i} X_{overallBA,i} + \\ & \beta_{13} X_{cwd,j} X_{propHost,i} X_{PipoHeight,i} + \\ & \mathcal{GP}_j(x_i, y_i) \end{aligned} \tag{1}$$

542 Where y_i is the number of dead trees in cell i , n_i is the sum of the dead trees (assumed to be ponderosa pine)
543 and live ponderosa pine trees in cell i , π_i is the probability of ponderosa pine tree mortality in cell i , p is the
544 probability of there being zero dead trees in a cell arising as a result of an independent, unmodeled process,
545 $X_{cwd,j}$ is the z-score of CWD for site j , $X_{propHost,i}$ is the scaled proportion of trees that are ponderosa pine
546 in cell i , $X_{PipoHeight,i}$ is the scaled mean height of ponderosa pine trees in cell i , $X_{overallDensity,i}$ is the scaled
547 density of all trees in cell i , $X_{overallBA,i}$ is the scaled basal area of all trees in cell i , x_i and y_i are the x- and
548 y- coordinates of the centroid of the cell in an EPSG3310 coordinate reference system, and \mathcal{GP}_j represents
549 the exact Gaussian process describing the spatial covariance between cells at site j .

550 We fit this model using the `brms` package¹⁰⁷ which implements the No U-Turn Sampler extension to the
551 Hamiltonian Monte Carlo algorithm¹⁰⁸ in the Stan programming language.¹⁰⁹ We used 4 chains with 5000
552 iterations each (2000 warmup, 3000 samples), and confirmed chain convergence by ensuring all `Rhat` values
553 were less than 1.1¹¹⁰ and that the bulk and tail effective sample sizes (ESS) for each estimated parameter
554 were greater than 100 times the number of chains (i.e., greater than 400 in our case). We used posterior
555 predictive checks to visually confirm model performance by overlaying the density curves of the predicted
556 number of dead trees per cell over the observed number.¹¹¹ For the posterior predictive checks, we used 50
557 random samples from the model fit to generate 50 density curves and ensured curves were centered on the
558 observed distribution, paying special attention to model performance at capturing counts of zero.

559 **Data availability**

560 All field and drone data processed for this study are available via the Open Science Framework at <https://doi.org/10.17605/OSF.IO/3CWF9>.¹¹² The administrative boundaries file for the USDA Forest Service (S_USA.AdministrativeForest.shp) can be found at <https://data.fs.usda.gov/geodata/edw/datasets.php?dsetCategory=boundaries>. The 2014 version of the 1981-2010 thirty-year historic average climatic water deficit data (cwd1981_2010_ave_HST_1550861123.tif) can be found on the California Climate Commons at <http://climate.calcommons.org/dataset/2014-CA-BCM>. The dataset representing ponderosa pine geolocations derived from herbaria records (California_Species_clean_All_epsg_3310.csv) can be found at <https://doi.org/10.6078/D16K5W>.¹¹³ The vector file representing Jepson geographic subdivisions of California and used to define the Sierra Nevada region can be requested at <https://ucjeps.berkeley.edu/eflora/geography.html>.

570 **Code availability**

571 Statistical analyses were performed using the `brms` packages. With the exception of the SfM software (Pix4Dmapper Cloud) and the GIS software QGIS, all data carpentry and analyses were performed using R.¹¹⁴ All code used to generate the results from this study are available via GitHub at <https://github.com/mikoontz/local-structure-wpb-severity> and is mirrored on the Open Science Framework at <https://doi.org/10.17605/OSF.IO/WPK5Z>.¹¹⁵

576 **Acknowledgements**

577 We gratefully acknowledge funding from the USDA Forest Service Western Wildlands Environmental Threat Assessment Center (WWETAC) and the Pacific Southwest Research Station Climate Change Competitive Grant Program. We thank Connie Millar for comments and guidance during the development of this project, Victoria Scholl for helpful discussions regarding remotely-sensed data product levels, and Derek Young for helpful discussions while revising this manuscript. We also thank Meagan Oldfather for her role as visual observer during drone flights. We gratefully acknowledge Pix4D, which provided free cloud infrastructure for much of the Structure from Motion photogrammetry processing. Finally, we thank the Open Science Framework for facilitating the public access to our complete dataset.

585 **Author contributions**

586 Author contributions are defined using the Contributor Roles Taxonomy (CRediT; <https://casrai.org/credit/>).
587 Conceptualization: MJK, AML, CJF, MPN, LAM; Data curation: MJK; Formal analysis: MJK; Funding

588 acquisition: MJK, MPN, CJF, AML; Investigation: MJK, LAM, CJF; Methodology: MJK, AML; Project
589 administration: MJK; Resources: MJK, MPN, AML; Software: MJK; Supervision: MJK, MPN, AML;
590 Validation: MJK; Visualization: MJK; Writing – original draft: MJK; Writing – review and editing: MJK,
591 AML, CJF, MPN, LAM

592 **Competing interests**

593 The authors declare no competing interests.

References

- 594 1. USDAFS. Press Release: Survey finds 18 million trees died in California in 2018. https://www.fs.usda.gov/Internet/FSE_DOCUMENTS/FSEPRD609321.pdf (2019).
- 595 2. Griffin, D. & Anchukaitis, K. J. How unusual is the 2012-2014 California drought? *Geophysical Research Letters* **41**, 9017–9023 (2014).
- 596 3. Robeson, S. M. Revisiting the recent California drought as an extreme value. *Geophysical Research Letters* **42**, 6771–6779 (2015).
- 597 4. Asner, G. P. *et al.* Progressive forest canopy water loss during the 2012-2015 California drought. *Proceedings of the National Academy of Sciences* **113**, E249–E255 (2016).
- 598 5. Brodrick, P. G. & Asner, G. P. Remotely sensed predictors of conifer tree mortality during severe drought. *Environ. Res. Lett.* **12**, 115013 (2017).
- 599 6. Fettig, C. J. Chapter 2: Forest health and bark beetles. in *Managing Sierra Nevada Forests. PSW-GTR-237* (USDA Forest Service, 2012).
- 600 7. Kolb, T. E. *et al.* Observed and anticipated impacts of drought on forest insects and diseases in the United States. *Forest Ecology and Management* **380**, 321–334 (2016).
- 601 8. Waring, R. H. & Pitman, G. B. Modifying lodgepole pine stands to change susceptibility to mountain pine beetle attack. *Ecology* **66**, 889–897 (1985).
- 602 9. Restaino, C. *et al.* Forest structure and climate mediate drought-induced tree mortality in forests of the Sierra Nevada, USA. *Ecological Applications* **0**, e01902 (2019).
- 603 10. USDAFS. Press Release: Record 129 million dead trees in California. https://www.fs.usda.gov/Internet/FSE_DOCUMENTS/fseprd566303.pdf (2017).
- 604 11. Young, D. J. N. *et al.* Long-term climate and competition explain forest mortality patterns under extreme drought. *Ecology Letters* **20**, 78–86 (2017).
- 605 12. Raffa, K. F. *et al.* Cross-scale drivers of natural disturbances prone to anthropogenic amplification: The dynamics of bark beetle eruptions. *BioScience* **58**, 501–517 (2008).
- 606 13. Boone, C. K., Aukema, B. H., Bohlmann, J., Carroll, A. L. & Raffa, K. F. Efficacy of tree defense physiology varies with bark beetle population density: A basis for positive feedback in eruptive species. *Can. J. For. Res.* **41**, 1174–1188 (2011).

- 622 14. Fettig, C. J., Mortenson, L. A., Bulaon, B. M. & Foulk, P. B. Tree mortality following drought in the
623 central and southern Sierra Nevada, California, U.S. *Forest Ecology and Management* **432**, 164–178 (2019).
- 624 15. Stephenson, N. L., Das, A. J., Ampersee, N. J. & Bulaon, B. M. Which trees die during drought? The
625 key role of insect host-tree selection. *Journal of Ecology* **75**, 2383–2401 (2019).
- 626 16. Senf, C., Campbell, E. M., Pflugmacher, D., Wulder, M. A. & Hostert, P. A multi-scale analysis of
627 western spruce budworm outbreak dynamics. *Landscape Ecol* **32**, 501–514 (2017).
- 628 17. Seidl, R. *et al.* Small beetle, large-scale drivers: How regional and landscape factors affect outbreaks of
629 the European spruce bark beetle. *J Appl Ecol* **53**, 530–540 (2016).
- 630 18. Fettig, C. J. Native bark beetles and wood borers in Mediterranean forests of California. in *Insects and*
631 *diseases of Mediterranean Forest systems* 499–528 (Springer International Publishing, 2016).
- 632 19. Raffa, K. F. & Berryman, A. A. The role of host plant resistance in the colonization behavior and ecology
633 of bark beetles (Coleoptera: Scolytidae). *Ecological Monographs* **53**, 27–49 (1983).
- 634 20. Logan, J. A., White, P., Bentz, B. J. & Powell, J. A. Model analysis of spatial patterns in mountain pine
635 beetle outbreaks. *Theoretical Population Biology* **53**, 236–255 (1998).
- 636 21. Wallin, K. F. & Raffa, K. F. Feedback between individual host selection behavior and population dynamics
637 in an eruptive herbivore. *Ecological Monographs* **74**, 101–116 (2004).
- 638 22. Franceschi, V. R., Krokene, P., Christiansen, E. & Krekling, T. Anatomical and chemical defenses of
639 conifer bark against bark beetles and other pests. *New Phytologist* **167**, 353–376 (2005).
- 640 23. Raffa, K. F., Grégoire, J.-C. & Staffan Lindgren, B. Natural history and ecology of bark beetles. in *Bark*
641 *Beetles* 1–40 (Elsevier, 2015). doi:10.1016/B978-0-12-417156-5.00001-0.
- 642 24. Bentz, B. J. *et al.* Climate change and bark beetles of the western United States and Canada: Direct and
643 indirect effects. *BioScience* **60**, 602–613 (2010).
- 644 25. DeRose, R. J. & Long, J. N. Drought-driven disturbance history characterizes a southern Rocky Mountain
645 subalpine forest. *Can. J. For. Res.* **42**, 1649–1660 (2012).
- 646 26. Hart, S. J., Veblen, T. T., Schneider, D. & Molotch, N. P. Summer and winter drought drive the initiation
647 and spread of spruce beetle outbreak. *Ecology* **98**, 2698–2707 (2017).
- 648 27. Netherer, S., Panassiti, B., Pennerstorfer, J. & Matthews, B. Acute drought Is an important driver of
649 bark beetle infestation in Austrian Norway spruce stands. *Front. For. Glob. Change* **2**, (2019).

- 650 28. Kaiser, K. E., McGlynn, B. L. & Emanuel, R. E. Ecohydrology of an outbreak: Mountain pine beetle
651 impacts trees in drier landscape positions first. *Ecohydrology* **6**, 444–454 (2013).
- 652 29. Marini, L. *et al.* Climate drivers of bark beetle outbreak dynamics in Norway spruce forests. *Ecography*
653 **40**, 1426–1435 (2017).
- 654 30. Sambaraju, K. R., Carroll, A. L. & Aukema, B. H. Multiyear weather anomalies associated with range
655 shifts by the mountain pine beetle preceding large epidemics. *Forest Ecology and Management* **438**, 86–95
656 (2019).
- 657 31. Hayes, C. J., Fettig, C. J. & Merrill, L. D. Evaluation of multiple funnel traps and stand characteristics
658 for estimating western pine beetle-caused tree mortality. *Journal of Economic Entomology* **102**, 2170–2182
659 (2009).
- 660 32. Thistle, H. W. *et al.* Surrogate pheromone plumes in three forest trunk spaces: Composite statistics and
661 case studies. *Forest Science* **50**, (2004).
- 662 33. Miller, J. M. & Keen, F. P. *Biology and control of the western pine beetle: A summary of the first fifty*
663 *years of research.* (US Department of Agriculture, 1960).
- 664 34. Chubaty, A. M., Roitberg, B. D. & Li, C. A dynamic host selection model for mountain pine beetle,
665 *Dendroctonus ponderosae* Hopkins. *Ecological Modelling* **220**, 1241–1250 (2009).
- 666 35. Graf, M., Reid, M. L., Aukema, B. H. & Lindgren, B. S. Association of tree diameter with body size and
667 lipid content of mountain pine beetles. *The Canadian Entomologist* **144**, 467–477 (2012).
- 668 36. Geiszler, D. R. & Gara, R. I. Mountain pine beetle attack dynamics in lodgepole pine. in *Theory and*
669 *Practice of Mountain Pine Beetle Management in Lodgepole Pine Forests: Symposium Proceedings.* A. A.
670 *Berryman, G. D. Amman and R. W. Stark (Eds)* (1978).
- 671 37. Klein, W. H., Parker, D. L. & Jensen, C. E. Attack, emergence, and stand depletion trends of the
672 mountain pine beetle in a lodgepole pine stand during an outbreak. *Environ Entomol* **7**, 732–737 (1978).
- 673 38. Mitchell, R. G. & Preisler, H. K. Analysis of spatial patterns of lodgepole pine attacked by outbreak
674 populations of the mountain pine beetle. *Forest Science* **37**, 1390–1408 (1991).
- 675 39. Preisler, H. K. Modelling spatial patterns of trees attacked by bark-beetles. *Applied Statistics* **42**, 501
676 (1993).
- 677 40. Jactel, H. & Brockerhoff, E. G. Tree diversity reduces herbivory by forest insects. *Ecology Letters* **10**,
678 835–848 (2007).

- 679 41. Faccoli, M. & Bernardinelli, I. Composition and elevation of spruce forests affect susceptibility to bark
680 beetle attacks: Implications for forest management. *Forests* **5**, 88–102 (2014).
- 681 42. Berryman, A. A. Population dynamics of bark beetles. in *Bark Beetles in North American Conifers: A*
682 *System for the Study of Evolutionary Biology* 264–314 (1982).
- 683 43. Fettig, C. J. *et al.* The effectiveness of vegetation management practices for prevention and control of
684 bark beetle infestations in coniferous forests of the western and southern United States. *Forest Ecology and*
685 *Management* **238**, 24–53 (2007).
- 686 44. Moeck, H. A., Wood, D. L. & Lindahl, K. Q. Host selection behavior of bark beetles (Coleoptera:
687 Scolytidae) attacking *Pinus ponderosa*, with special emphasis on the western pine beetle, *Dendroctonus*
688 *brevicomis*. *Journal of Chemical Ecology* **7**, 49–83 (1981).
- 689 45. Evenden, M. L., Whitehouse, C. M. & Sykes, J. Factors influencing flight capacity of the mountain pine
690 beetle (Coleoptera: Curculionidae: Scolytinae). *Environ Entomol* **43**, 187–196 (2014).
- 691 46. Raffa, K. F. & Berryman, A. A. Accumulation of monoterpenes and associated volatiles following
692 inoculation of grand fir with a fungus transmitted by the fir engraver, *Scolytus ventralis* (Coleoptera:
693 Scolytidae). *The Canadian Entomologist* **114**, 797–810 (1982).
- 694 47. Anderegg, W. R. L. *et al.* Tree mortality from drought, insects, and their interactions in a changing
695 climate. *New Phytologist* **208**, 674–683 (2015).
- 696 48. Kane, V. R. *et al.* Assessing fire effects on forest spatial structure using a fusion of Landsat and airborne
697 LiDAR data in Yosemite National Park. *Remote Sensing of Environment* **151**, 89–101 (2014).
- 698 49. Larson, A. J. & Churchill, D. Tree spatial patterns in fire-frequent forests of western North America,
699 including mechanisms of pattern formation and implications for designing fuel reduction and restoration
700 treatments. *Forest Ecology and Management* **267**, 74–92 (2012).
- 701 50. Morris, J. L. *et al.* Managing bark beetle impacts on ecosystems and society: Priority questions to
702 motivate future research. *Journal of Applied Ecology* **54**, 750–760 (2017).
- 703 51. Shiklomanov, A. N. *et al.* Enhancing global change experiments through integration of remote-sensing
704 techniques. *Frontiers in Ecology and the Environment* **0**, (2019).
- 705 52. Jeronimo, S. M. A. *et al.* Forest structure and pattern vary by climate and landform across active-fire
706 landscapes in the montane Sierra Nevada. *Forest Ecology and Management* **437**, 70–86 (2019).
- 707 53. Roussel, J.-R., Auty, D., De Boissieu, F. & Meador, A. S. *lidR: Airborne LiDAR data manipulation and*

- 708 *visualization for forestry applications*. (2019).
- 709 54. McDowell, N. *et al.* Mechanisms of plant survival and mortality during drought: Why do some plants
710 survive while others succumb to drought? *New Phytologist* **178**, 719–739 (2008).
- 711 55. Seybold, S. J. *et al.* Management of western North American bark beetles with semiochemicals. *Annual*
712 *Review of Entomology* **63**, 407–432 (2018).
- 713 56. Fettig, C. J., McKelvey, S. R. & Huber, D. P. W. Nonhost angiosperm volatiles and Verbenone disrupt
714 response of western pine beetle, *Dendroctonus brevicomis* (Coleoptera: Scolytidae), to attractant-baited traps.
715 *ecen* **98**, 2041–2048 (2005).
- 716 57. Fettig, C. J., Dabney, C. P., McKelvey, S. R. & Huber, D. P. W. Nonhost angiosperm volatiles and
717 verbenone protect individual ponderosa pines from attack by western pine beetle and red turpentine beetle
718 (Coleoptera: Curculionidae, Scolytinae). *west j appl for* **23**, 40–45 (2008).
- 719 58. Fettig, C. J. *et al.* Efficacy of ‘Verbenone Plus’ for protecting ponderosa pine trees and stands from
720 *Dendroctonus brevicomis* (Coleoptera: Curculionidae) attack in British Columbia and California. *J Econ*
721 *Entomol* **105**, 1668–1680 (2012).
- 722 59. Oliver, W. W. Is self-thinning in ponderosa pine ruled by *Dendroctonus* bark beetles? in *Forest health*
723 *through silviculture: Proceedings of the 1995 National Silviculture Workshop* 6 (1995).
- 724 60. Fettig, C. & McKelvey, S. Resiliency of an Interior Ponderosa Pine Forest to Bark Beetle Infestations
725 Following Fuel-Reduction and Forest-Restoration Treatments. *Forests* **5**, 153–176 (2014).
- 726 61. Fettig, C. J. & Hilszczański, J. Management strategies for bark beetles in conifer forests. in *Bark Beetles*
727 555–584 (Elsevier, 2015). doi:10.1016/B978-0-12-417156-5.00014-9.
- 728 62. Chesson, P. Mechanisms of maintenance of species diversity. *Annual Review of Ecology and Systematics*
729 **31**, 343–366 (2000).
- 730 63. Fricker, G. A. *et al.* More than climate? Predictors of tree canopy height vary with scale in complex
731 terrain, Sierra Nevada, CA (USA). *Forest Ecology and Management* **434**, 142–153 (2019).
- 732 64. Ma, S., Concilio, A., Oakley, B., North, M. & Chen, J. Spatial variability in microclimate in a mixed-conifer
733 forest before and after thinning and burning treatments. *Forest Ecology and Management* **259**, 904–915
734 (2010).
- 735 65. Stovall, A. E. L., Shugart, H. & Yang, X. Tree height explains mortality risk during an intense drought.
736 *Nature Communications* **10**, 1–6 (2019).

- 737 66. Stephenson, N. L. & Das, A. J. Height-related changes in forest composition explain increasing tree
738 mortality with height during an extreme drought. *Nature Communications* **11**, 3402 (2020).
- 739 67. Stovall, A. E. L., Shugart, H. H. & Yang, X. Reply to ‘Height-related changes in forest composition
740 explain increasing tree mortality with height during an extreme drought’. *Nature Communications* **11**, 3401
741 (2020).
- 742 68. Person, H. L. Tree selection by the western pine beetle. *J for* **26**, 564–578 (1928).
- 743 69. Person, H. L. Theory in explanation of the selection of certain trees by the western pine beetle. *J for* **29**,
744 696–699 (1931).
- 745 70. Pile, L. S., Meyer, M. D., Rojas, R., Roe, O. & Smith, M. T. Drought impacts and compounding mortality
746 on forest trees in the southern Sierra Nevada. *Forests* **10**, 237 (2019).
- 747 71. Frey, J., Kovach, K., Stemmler, S. & Koch, B. UAV photogrammetry of forests as a vulnerable process.
748 A sensitivity analysis for a structure from motion RGB-image pipeline. *Remote Sensing* **10**, 912 (2018).
- 749 72. James, M. R. & Robson, S. Mitigating systematic error in topographic models derived from UAV and
750 ground-based image networks. *Earth Surface Processes and Landforms* **39**, 1413–1420 (2014).
- 751 73. Gray, P. C. *et al.* A convolutional neural network for detecting sea turtles in drone imagery. *Methods in*
752 *Ecology and Evolution* **10**, 345–355 (2019).
- 753 74. Millar, C. I., Stephenson, N. L. & Stephens, S. L. Climate change and forests of the future: Managing in
754 the face of uncertainty. *Ecological Applications* **17**, 2145–2151 (2007).
- 755 75. Vose, J. M. *et al.* Forests. In *Impacts, Risks, and Adaptation in the United States: The Fourth National*
756 *Climate Assessment, Volume II [Reidmiller, D. R., C. W. Avery, D. R. Easterling, K. E. Kunkel, K. L. M.*
757 *Lewis, T. K. Maycock, and B. C. Stewart (eds.)]*. 232–267 <https://nca2018.globalchange.gov/chapter/6/>
758 (2018) doi:10.7930/NCA4.2018.CH6.
- 759 76. Bedard, W. D. *et al.* Western pine beetle: Field response to its sex pheromone and a synergistic host
760 terpene, myrcene. *Science* **164**, 1284–1285 (1969).
- 761 77. Byers, J. A. & Wood, D. L. Interspecific inhibition of the response of the bark beetles, *Dendroctonus*
762 *brevicomis* and *Ips paraconfusus*, to their pheromones in the field. *J Chem Ecol* **6**, 149–164 (1980).
- 763 78. Shepherd, W. P., Huber, D. P. W., Seybold, S. J. & Fettig, C. J. Antennal responses of the western pine
764 beetle, *Dendroctonus brevicomis* (Coleoptera: Curculionidae), to stem volatiles of its primary host, *Pinus*
765 *ponderosa*, and nine sympatric nonhost angiosperms and conifers. *Chemoecology* **17**, 209–221 (2007).

- 766 79. DJI. Zenmuse X3 - Creativity Unleashed. *DJI Official* <https://www.dji.com/zenmuse-x3/info> (2015).
- 767 80. Micasense. MicaSense. [https://support.micasense.com/hc/en-us/articles/215261448-RedEdge-User-](https://support.micasense.com/hc/en-us/articles/215261448-RedEdge-User-Manual-PDF-Download-)
768 [Manual-PDF-Download-](https://support.micasense.com/hc/en-us/articles/215261448-RedEdge-User-Manual-PDF-Download-) (2015).
- 769 81. DJI. DJI - The World Leader in Camera Drones/Quadcopters for Aerial Photography. *DJI Official*
770 <https://www.dji.com/matrice100/info> (2015).
- 771 82. Wyngaard, J. *et al.* Emergent challenges for science sUAS data management: Fairness through community
772 engagement and best practices development. *Remote Sensing* **11**, 1797 (2019).
- 773 83. Rouse, W., Haas, R. H., Deering, W. & Schell, J. A. *Monitoring the vernal advancement and retrogradation*
774 *(green wave effect) of natural vegetation.* (1973).
- 775 84. DronesMadeEasy. Map Pilot for DJI on iOS. *App Store* [https://itunes.apple.com/us/app/map-pilot-for-](https://itunes.apple.com/us/app/map-pilot-for-dji/id1014765000?mt=8)
776 [dji/id1014765000?mt=8](https://itunes.apple.com/us/app/map-pilot-for-dji/id1014765000?mt=8) (2018).
- 777 85. Farr, T. G. *et al.* The shuttle radar topography mission. *Reviews of Geophysics* **45**, (2007).
- 778 86. Zhang, W. *et al.* An easy-to-use airborne LiDAR data filtering method based on cloth simulation. *Remote*
779 *Sensing* **8**, 501 (2016).
- 780 87. Hijmans, R. J. *et al.* *Raster: Geographic data analysis and modeling.* (2019).
- 781 88. Gitelson, A. & Merzlyak, M. N. Spectral reflectance changes associated with autumn senescence of
782 *Aesculus hippocastanum* L. And *Acer platanoides* L. Leaves. Spectral features and relation to chlorophyll
783 estimation. *Journal of Plant Physiology* **143**, 286–292 (1994).
- 784 89. Coops, N. C., Johnson, M., Wulder, M. A. & White, J. C. Assessment of QuickBird high spatial resolution
785 imagery to detect red attack damage due to mountain pine beetle infestation. *Remote Sensing of Environment*
786 **103**, 67–80 (2006).
- 787 90. Clevers, J. G. P. W. & Gitelson, A. A. Remote estimation of crop and grass chlorophyll and nitrogen
788 content using red-edge bands on Sentinel-2 and -3. *International Journal of Applied Earth Observation and*
789 *Geoinformation* **23**, 344–351 (2013).
- 790 91. Li, W., Guo, Q., Jakubowski, M. K. & Kelly, M. A new method for segmenting individual trees from the
791 LiDAR point cloud. *Photogrammetric Engineering & Remote Sensing* **78**, 75–84 (2012).
- 792 92. Jakubowski, M. K., Li, W., Guo, Q. & Kelly, M. Delineating individual trees from LiDAR data: A
793 comparison of vector- and raster-based segmentation approaches. *Remote Sensing* **5**, 4163–4186 (2013).

- 794 93. Shin, P., Sankey, T., Moore, M. & Thode, A. Evaluating unmanned aerial vehicle images for estimating
795 forest canopy fuels in a ponderosa pine stand. *Remote Sensing* **10**, 1266 (2018).
- 796 94. Roussel, J.-R. *lidRplugins: Extra functions and algorithms for lidR package.* (2019).
- 797 95. Eysn, L. *et al.* A benchmark of LiDAR-based single tree detection methods using heterogeneous forest
798 data from the alpine space. *Forests* **6**, 1721–1747 (2015).
- 799 96. Vega, C. *et al.* PTrees: A point-based approach to forest tree extraction from LiDAR data. *International*
800 *Journal of Applied Earth Observation and Geoinformation* **33**, 98–108 (2014).
- 801 97. Plowright, A. *ForestTools: Analyzing remotely sensed forest data.* (2018).
- 802 98. Pau, G., Fuchs, F., Sklyar, O., Boutros, M. & Huber, W. EBImage: An R package for image processing
803 with applications to cellular phenotypes. *Bioinformatics* **26**, 979–981 (2010).
- 804 99. Meyer, F. & Beucher, S. Morphological segmentation. *Journal of Visual Communication and Image*
805 *Representation* **1**, 21–46 (1990).
- 806 100. Hunziker, P. *Velox: Fast raster manipulation and extraction.* (2017).
- 807 101. Kuhn, M. Building predictive models in R using the caret package. *Journal of Statistical Software* **28**,
808 1–26 (2008).
- 809 102. Wang, Y. *et al.* Is field-measured tree height as reliable as believed A comparison study of tree height
810 estimates from field measurement, airborne laser scanning and terrestrial laser scanning in a boreal forest.
811 *ISPRS Journal of Photogrammetry and Remote Sensing* **147**, 132–145 (2019).
- 812 103. Stephenson, N. Actual evapotranspiration and deficit: Biologically meaningful correlates of vegetation
813 distribution across spatial scales. *Journal of Biogeography* **25**, 855–870 (1998).
- 814 104. Flint, L. E., Flint, A. L., Thorne, J. H. & Boynton, R. Fine-scale hydrologic modeling for regional
815 landscape applications: The California Basin Characterization Model development and performance. *Ecological*
816 *Processes* **2**, 25 (2013).
- 817 105. Millar, C. I. *et al.* Forest mortality in high-elevation whitebark pine (*Pinus albicaulis*) forests of eastern
818 California, USA: Influence of environmental context, bark beetles, climatic water deficit, and warming.
819 *Canadian Journal of Forest Research* **42**, 749–765 (2012).
- 820 106. Baldwin, B. G. *et al.* Species richness and endemism in the native flora of California. *American Journal*
821 *of Botany* **104**, 487–501 (2017).

- 822 107. Bürkner, P.-C. **brms**: An *R* package for bayesian multilevel models using *Stan*. *Journal of Statistical*
823 *Software* **80**, 1–28 (2017).
- 824 108. Hoffman, M. D. & Gelman, A. The No-U-Turn Sampler: Adaptively setting path lengths in Hamiltonian
825 Monte Carlo. *Journal of Machine Learning Research* **15**, 31 (2014).
- 826 109. Carpenter, B. *et al.* Stan: A Probabilistic Programming Language. *Journal of Statistical Software* **76**,
827 1–32 (2017).
- 828 110. Brooks, S. P. & Gelman, A. General methods for monitoring convergence of iterative simulations.
829 *Journal of Computational and Graphical Statistics* **7**, 434 (1998).
- 830 111. Gabry, J., Simpson, D., Vehtari, A., Betancourt, M. & Gelman, A. Visualization in Bayesian workflow.
831 *Journal of the Royal Statistical Society: Series A (Statistics in Society)* **182**, 389–402 (2019).
- 832 112. Koontz, M. J., Latimer, A. M., Mortenson, L. A., Fettig, C. J. & North, M. P. Drone-derived data
833 supporting "Cross-scale interaction of host tree size and climatic water deficit governs bark beetle-induced
834 tree mortality". (2020) doi:10.17605/OSF.IO/3CWF9.
- 835 113. Baldwin, B. G. *et al.* Master spatial file for native California vascular plants used by Baldwin *et al.*
836 (2017 Amer. J. Bot.). *American Journal of Botany* **3** (2017).
- 837 114. R Core Team. *R: A language and environment for statistical computing*. (R Foundation for Statistical
838 Computing, 2018).
- 839 115. Koontz, M. J., Latimer, A. M., Mortenson, L. A., Fettig, C. J. & North, M. P. Local-structure-wpb-
840 severity. (2019) doi:10.17605/OSF.IO/WPK5Z.